2011 American Control Conference
on O'Farrell Street, San Francisco, CA, USA
June 29 - July 01, 2011

6DOF Flight Control of Fixed-Wing Aircraft by Trajectory Linearization

Tony M. Adami, *Member, AIAA,* and J. Jim Zhu, *Senior Member, IEEE, Senior Member, AIAA*

Abstract— **In this paper, Trajectory Linearization Control (TLC) is used to design a six degree-of-freedom, autonomous, trajectory-tracking controller for a fixed-wing vehicle dynamics model. TLC combines an open-loop dynamic inverse of the plant dynamics with a closed-loop tracking-error regulator that accounts for model mismatch, disturbances, and excitation of internal dynamics. Feedback gains are obtained symbolically as a function of the nominal trajectory, thus avoiding the use of gain scheduling, and enabling operation across the full flight-envelope without the need for mode-switching. The design method is presented, and trajectory-tracking simulation results are given for a climbing, bank-to-turn maneuver.**

I. Introduction

Due to the highly nonlinear and time-varying nature of flight dynamics in maneuvering trajectory-tracking, nonlinear solutions have been heavily researched in the past several decades. Linear time-invariant (LTI) methods have well-known limitations, and conventional autopilots are typically limited to point-to-point flight plans (waypoint tracking), multiple-mode operation, and specially pre-defined trajectories. There are many factors currently driving the need for full-envelope, autonomous flight control systems. The rapidly-growing use of unmanned air vehicles (UAV) has focused attention on the need for autonomous attitude and trajectory tracking [1]. For air vehicles, loss-of-control remains the number one cause for loss-of-vehicle mishaps for commercial flights [2]. Plans for the next generation airspace will rely heavily on effective, affordable solutions to increased air traffic density, as well as stricter safety requirements that can be validated and certified. Advanced guidance and control architectures and algorithms are needed to cope with off-nominal flight conditions and vehicle subsystem failures. Military aircraft pose significant challenges, including fast-varying and unsteady systems, aggressive maneuvers, and rapidly changing environments. Advances in airframe design and materials driven by pressure and temperature requirements have led to relatively lightweight aircraft with significant flex modes. Vehicles in this class exhibit heavy coupling between aerodynamics, propulsion, and structural modes that takes the control problem a significant step further [3].

Gain scheduling has been used toward trajectory tracking for systems with dynamics that change sufficiently slowly, and that do not encounter highly-variable flight conditions. Controllers are designed at multiple operating points, and can be scheduled along a trajectory on, for example, altitude and Mach number. Some main results on gain scheduling are presented in [4,5], and additional theoretical developments are presented in [6]. Linear Parameter-Varying (LPV) system theory is described in [7] as a natural extension of gain scheduling, and applications include control of a longitudinal dynamics model of the Lockheed P2V-7 aircraft [8], and missile autopilots in conjunction with H^{∞} [9].

Modern nonlinear control techniques such as feedback linearization and dynamic inversion (DI) have been effective for some classes of vehicles by cancelling the nonlinearity via a coordinate transformation and state feedback, or by constructing a dynamic inverse of the nonlinear plant [10-12]. LTI tracking-error dynamics can be formulated after the nonlinear cancellation, and controlled by LTI controllers. A drawback of this type of control scheme is that the nonlinearity cancellation is accomplished within the feedback control loop, and therefore imperfect cancellation due to sensor dynamics or modeling errors would result in nonlinear dynamics that cannot be adequately compensated by the LTI controller.

In Ref. [13], Eigenstructure Assignment [14], DI, and μ-Synthesis [15-16] are compared in detail. Adaptive Control is described in [17], and flight control applications often combine adaptation with other tools such as Backstepping and Neural Networks [18-20], Sliding Mode Control [21], and DI [22]. An alternative approach to trajectory-tracking is path-following control, a method that reduces the relative importance of the trajectory's time-dimension [23].

Nonlinear tracking and decoupling control by trajectory linearization can be viewed as ideal, gain-scheduled controllers designed at every point on the trajectory [24]. The trajectory command is embedded in the controller gains by analytical (symbolic) design. Therefore, TLC provides robust stability without slowly-varying constraints on the command trajectories, interpolation of controller gains, or trajectory-dependent redesigns. TLC approximately cancels the plant nonlinearity in an open-loop fashion. This provides

Manuscript received September 27, 2010. This work was supported in part by NASA Fundamental Aeronautics, Subsonic Fixed Wing Program, Payload Directed Flight Project. Tony Adami and Jim Zhu would like to express sincere gratitude to NASA Ames Research Center for funding this work. Special thanks are due to Corey Ippolito, Diane Acosta, Joe Totah, and John Kaneshige.

T. M. Adami is with the Ohio University Avionics Engineering Center, Stocker 212, Athens, OH, 45701, USA: 740-593-1590; fax: 740-593-1604; (e-mail: adami@ohio.edu).

J. J. Zhu is with the School of Electrical Engineering and Computer Science, Ohio University, Athens, OH, 45701, USA (e-mail: zhuj@ohio.edu).

agile tracking response and reduced tracking-error that facilitates linearization of the nonlinear, time-varying tracking-error dynamics for linear time-varying (LTV) stabilization using PD-spectral theory [25,26]. Exponential stability of the tracking-error signal is thereby guaranteed [31]. An introduction to PD-Spectral theory is given in [32], and the TLC concept is illustrated in Figure 1.

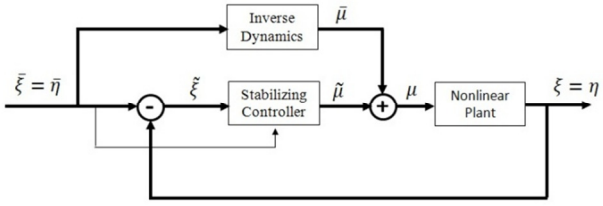

Figure 1. Trajectory Linearization concept

Figure 2 shows some of the platforms that have been simulated and/or tested previously, and the models and TLC controller designs are described in [27-30]. The X-33 model included the full range of aerodynamics, though the design was limited to 3DOF attitude control. Both a 3DOF and a 6DOF design have been synthesized for the Delta-UFO, but this type of tri-propeller hovercraft vehicle is a slow-flyer that is not subject to aerodynamics beyond parasitic drag. The longitudinal dynamics model of a hypersonic scramjet developed at Wright Patterson Air Force Base fully accounts for aerodynamics, but does not include lateral/directional motion (note that the vehicle depicted in the figure is the NASA X-43A, a prototype vehicle similar in concept). The design procedure had not yet addressed an aircraft model with both significant aerodynamic effects and full freedom of motion. There remained a need to develop a 6DOF flight control system for fixed-wing vehicles experiencing the full-range of aerodynamics, and over the full flight-envelope.

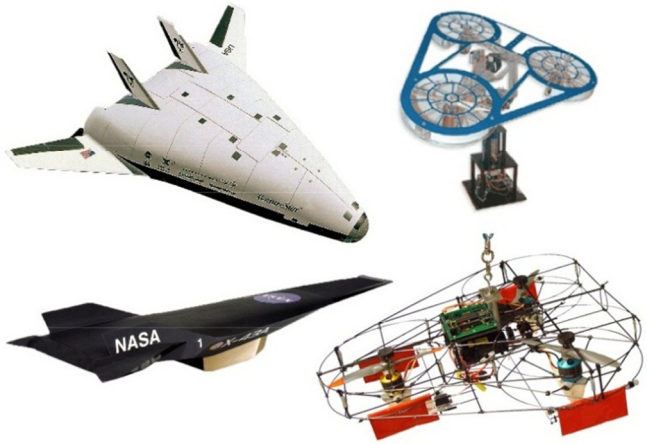

Figure 2: Clockwise from upper left: NASA X-33 Launch Vehicle, Quansar 3DOF UFO, 6DOF Delta-UFO, NASA X-43A.

In this paper, a 6DOF, trajectory-tracking TLC design for a single engine, general aviation aircraft model is presented, including a control allocation strategy using force/torque-model inversion to calculate control effector settings. Simulation results are given for a nominal, climbing, bank-to-turn maneuver.

II. Technical Preliminaries

An Earth-fixed reference frame will be considered an inertial frame for the purposes of this study. This is a good approximation for a Cessna 182 flying at 5000 ft, for example. The inertial frame is defined with positive x_e pointing due north, positive y_e pointing due east, and positive z_e pointing toward the center of the Earth. The origin is some fixed point on the Earth's surface that can be specified if necessary. The body-frame is defined with positive x_b pointing forward, along and parallel to the fuselage of the aircraft, and positive y_b aligned with the right wing and forming a 90° angle. z_b lies in the aircraft plane of symmetry and completes a right-handed coordinate system. The standard Euler angles ϕ, θ, and ψ relate the inertial and body-frame velocities as indicated in equation (7). The Local Horizon frame has its origin located at the aircraft center-of-gravity (cg), and remains aligned with the Earth-fixed frame so that the angles σ (bank), γ (flight path), and χ (heading) represent the aircraft's inertial attitude.

The forces and moments are approximated according to standard build-up methods using dimensionless coefficients obtained from the literature. Numerical values used for the current study have been adapted from [33], and the forces and moments are calculated according to equations (1) - (6).

$$D = QS\left(C_{D_\circ} + C_{D_\alpha}\alpha + C_{D_\beta}\beta + C_{D_{\delta a}}\delta_a + C_{D_{\delta e}}\delta_e + C_{D_{\delta r}}\delta_r\right) \quad (1)$$

$$Y = QS\left(C_{y_\beta}\beta + C_{y_{\delta r}}\delta_r + \frac{b}{2V_t}\left(C_{y_p}\hat{p} + C_{y_r}\hat{r}\right)\right) \quad (2)$$

$$L = QS\left(C_{L_\circ} + C_{L_\alpha}\alpha + C_{L_{\delta_e}}\delta_e + \frac{\bar{c}}{2V_t}\left(C_{L_{\dot{\alpha}}}\dot{\hat{\alpha}} + C_{L_q}\hat{q}\right)\right) \quad (3)$$

$$L_m = QSb\left(C_{l_\beta}\beta + C_{l_{\delta a}}\delta_a + C_{l_{\delta r}}\delta_r + \frac{b}{2V_t}\left(C_{l_p}\hat{p} + C_{y_r}\hat{r}\right)\right) \quad (4)$$

$$M_m = QS\bar{c}\left(C_{m_\circ} + C_{m_\alpha}\alpha + C_{m_{\delta e}}\delta_e + \frac{\bar{c}}{2V_t}\left(C_{m_{\dot{\alpha}}}\dot{\hat{\alpha}} + C_{m_q}\hat{q}\right)\right) \quad (5)$$

$$N_m = QSb\left(C_{n_\beta}\beta + C_{n_{\delta a}}\delta_a + C_{n_{\delta r}}\delta_r + \frac{b}{2V_t}\left(C_{n_p}\hat{p} + C_{n_r}\hat{r}\right)\right) \quad (6)$$

The thrust vector **T** is assumed parallel to x_b, passing through the cg so that $T_y=T_z=0$. The thrust force is therefore written simply as T, and is obtained using a proportional thrust law given by $T=T_{\max}\delta_T$. The twelve nonlinear, flat-earth equations of motion for a rigid-body are given in the body-fixed frame as equations (7) - (10). This formulation is convenient for obtaining the nominal states by matrix inversion or matrix algebra (a shorthand notation is used to write the state equations in which $S_\theta = \sin\theta$, $C_\psi = \cos\psi$, etc.). Note that **F** in equation (8) refers to the total applied force on the aircraft.

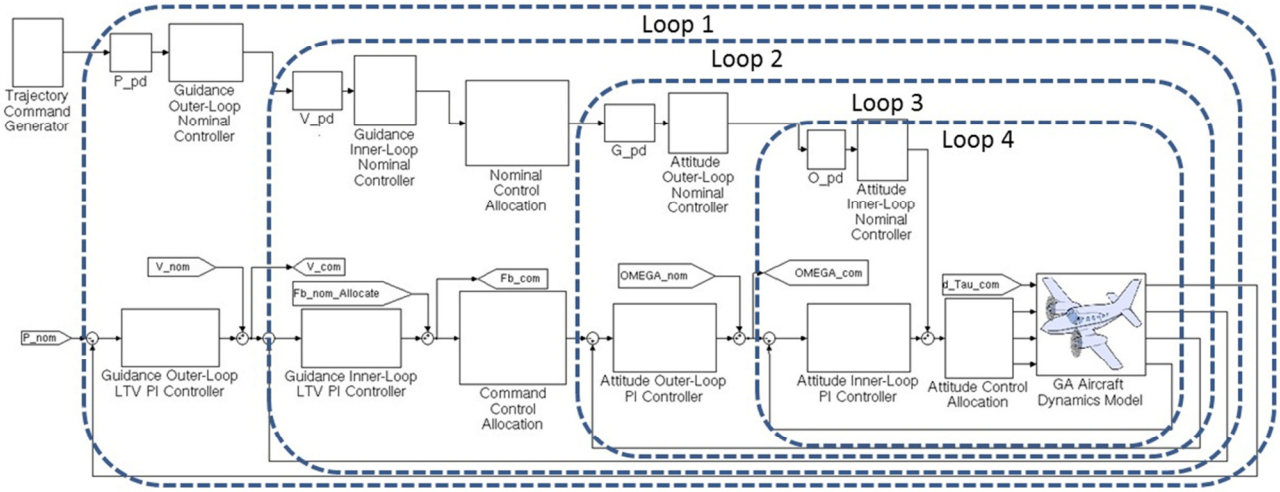

Figure 3. Simulink Implementation of 6DOF, TLC Controller

Translational Kinematics:

$$\begin{bmatrix}\dot{x}_e\\ \dot{y}_e\\ \dot{z}_e\end{bmatrix}=\begin{bmatrix}C_\theta C_\psi & S_\phi S_\theta C_\psi - C_\phi S_\psi & C_\phi S_\theta C_\psi + S_\phi S_\psi\\ C_\theta S_\psi & S_\phi S_\theta S_\psi + C_\phi C_\psi & C_\phi S_\theta S_\psi - S_\phi C_\psi\\ -S_\theta & S_\phi C_\theta & C_\phi C_\theta\end{bmatrix}\begin{bmatrix}u\\ v\\ w\end{bmatrix}$$

$$\boxed{\dot{\mathbf{P}} = B_1(\boldsymbol{\Gamma})\mathbf{V}} \tag{7}$$

Translational Dynamics:

$$\begin{bmatrix}\dot{u}\\ \dot{v}\\ \dot{w}\end{bmatrix}=\begin{bmatrix}0 & r & -q\\ -r & 0 & p\\ q & -p & 0\end{bmatrix}\begin{bmatrix}u\\ v\\ w\end{bmatrix}+\frac{1}{m}\begin{bmatrix}F_x\\ F_y\\ F_z\end{bmatrix}$$

$$\boxed{\dot{\mathbf{V}} = B_2(\boldsymbol{\Omega})\mathbf{V}+\frac{1}{m}\mathbf{F}} \tag{8}$$

Rotational Kinematics:

$$\begin{bmatrix}\dot{\phi}\\ \dot{\theta}\\ \dot{\psi}\end{bmatrix}=\begin{bmatrix}1 & S_\phi S_\theta/C_\theta & S_\theta C_\phi/C_\theta\\ 0 & C_\phi & -S_\phi\\ 0 & S_\phi/C_\theta & C_\phi/C_\theta\end{bmatrix}\begin{bmatrix}p\\ q\\ r\end{bmatrix}$$

$$\boxed{\dot{\boldsymbol{\Gamma}} = B_3(\boldsymbol{\Gamma})\boldsymbol{\Omega}} \tag{9}$$

Rotational Dynamics:

$$\begin{bmatrix}\dot{p}\\ \dot{q}\\ \dot{r}\end{bmatrix}=\begin{bmatrix}I^p_{pq}pq+I^p_{pr}qr\\ I^q_{pp}p^2+I^q_{rr}r^2+I^q_{pr}pr\\ I^r_{pq}pq+I^r_{qr}qr\end{bmatrix}+\begin{bmatrix}g^p_l & 0 & g^p_n\\ 0 & g^q_m & 0\\ g^r_l & 0 & g^r_n\end{bmatrix}\begin{bmatrix}L_m\\ M_m\\ N_m\end{bmatrix}$$

$$\boxed{\dot{\boldsymbol{\Omega}} = f_4(\boldsymbol{\Omega})+B_4\mathbf{T}_m} \tag{10}$$

The inertial constants in (10) are defined in the appendix.

III. 6DOF TLC Design for Fixed-Wing Vehicle

TLC combines nonlinear dynamic inversion as an open-loop controller with LTV feedback stabilization as a closed-loop controller as shown in Figure 1. The overall design consists of four loops as shown in Figure 3, each with a similar structure. The control allocation blocks perform force/torque model inversions and Euler-angle command calculations. A second-order pseudo-differentiator represented by the transfer function

$$G(s)=\frac{\omega_n^2 s}{s^2+2\zeta\omega_n s+\omega_n^2} \tag{11}$$

is implemented to realize the derivatives of the nominal states wherever it is needed, as well as to provide command filtering. The force commands are allocated in the guidance loop to the thrust coefficient δ_τ, and the virtual controls α (angle-of-attack) and β (sideslip angle). In the attitude loop, moment commands are allocated to the control surfaces δ_a (ailerons), δ_e (elevator), and δ_r (rudder).

1) 6DOF Trajectory Generation

The current implementation is driven by commanding flight-path and heading angles, as well as total velocity. The inertial and Local Horizon frames are related by

$$\begin{bmatrix}\dot{x}_{e,\mathrm{com}}\\ \dot{y}_{e,\mathrm{com}}\\ \dot{z}_{e,\mathrm{com}}\end{bmatrix}=\begin{bmatrix}V_{t,\mathrm{com}}\cos\gamma_{\mathrm{com}}\cos\chi_{\mathrm{com}}\\ V_{t,\mathrm{com}}\cos\gamma_{\mathrm{com}}\sin\chi_{\mathrm{com}}\\ -V_{t,\mathrm{com}}\sin\gamma_{\mathrm{com}}\end{bmatrix} \tag{12}$$

and it is straightforward to translate to position commands in inertial space. Using the TLC architecture, any set of vehicle states may be commanded, and a nominal trajectory for the overall state vector will be calculated and tracked.

2) Guidance Tracking Controller

The guidance tracking controller is shown as Loops 1 & 2 in Figure 3. The nominal force required to achieve the desired translational motion is calculated in the upper path, and feedback control is provided in the lower path. Outputs of the nominal and feedback controllers are $\bar{\mathbf{F}}_\mathrm{b}$ and $\mathbf{F}_{\mathrm{b,ctrl}}$ respectively.

Outer Loop Guidance Control

The nominal body velocity is obtained by dynamic inversion of the translational kinematics (7) at the current time step. The Euler rotation matrix is evaluated at $\bar{\mathbf{\Gamma}}_0$ as determined by the guidance allocation at the previous time step, and using (11) to calculate the nominal inertial velocity, the nominal body velocity is

$$\bar{\mathbf{V}} = B_1^{-1}\left(\bar{\mathbf{\Gamma}}_0\right)\dot{\bar{\mathbf{P}}}. \tag{13}$$

Feedback control is implemented by first defining the position error as $\mathbf{P}_{\text{err}} = \mathbf{P}_{\text{sens}} - \mathbf{P}_{\text{com}}$, and then linearizing along the nominal trajectory. The linearized, closed-loop error dynamics is written as

$$\dot{\mathbf{P}}_{\text{err}} = B_1\left(\bar{\mathbf{\Gamma}}_0\right)\mathbf{V}_{\text{ctrl}}, \tag{14}$$

and an LTV proportional-integral (PI) controller is synthesized using PD-spectral assignment (see Ref. [26] or [31] for details). As an illustration, consider the second-order LTV differential equation representing the desired closed-loop tracking error dynamics of the i$^{\text{th}}$ loop, j$^{\text{th}}$ channel given by

$$\ddot{e}_{ij} + \alpha_{ij2}(t)\dot{e}_{ij} + \alpha_{ij1}(t)e_{ij} = 0. \tag{15}$$

The PD-eigenvalues are chosen by specifying the desired closed-loop dynamics as

$$\alpha_{ij1}(t) = \omega_{n,j}^2(t), \quad \alpha_{ij2}(t) = \zeta_j\omega_{n,j}(t) - \frac{\dot{\omega}_{n,j}(t)}{\omega_{n,j}(t)} \tag{16}$$

where the ratio on the right side of (16) accounts for the time-varying, closed-loop dynamics. When this term is identically zero (i.e., ω_n are constant), the ordinary synthesis formula for second-order systems is obtained. It is noted that the current design employs time-invariant closed-loop tracking-error dynamics, and this simplifies the presentation from that standpoint. Time-varying dynamics can be used for adaptation or other purposes.

The PI control law is written next as

$$\mathbf{V}_{\text{ctrl}} = -\mathrm{K}_{\text{P1}}(t)\mathbf{P}_{\text{err}} - \mathrm{K}_{\text{I1}}(t)\int_{t_0}^{t}\mathbf{P}_{\text{err}}(\tau)\,d\tau \tag{17}$$

with the body velocity loop gain matrices obtained symbolically as

$$\mathrm{K}_{\text{I1}}(t) = -B_1^{-1}\left(\bar{\mathbf{\Gamma}}_0\right)A_{1\bullet 1}$$
$$= \begin{bmatrix} \alpha_{111}\mathrm{C}_{\bar{\theta}}\mathrm{C}_{\bar{\psi}} & \alpha_{121}\mathrm{C}_{\bar{\theta}}\mathrm{S}_{\bar{\psi}} & -\alpha_{131}\mathrm{S}_{\bar{\theta}} \\ \alpha_{111}\left(\mathrm{S}_{\bar{\phi}}\mathrm{S}_{\bar{\theta}}\mathrm{C}_{\bar{\psi}} - \mathrm{C}_{\bar{\phi}}\mathrm{S}_{\bar{\psi}}\right) & \alpha_{121}\left(\mathrm{S}_{\bar{\phi}}\mathrm{S}_{\bar{\theta}}\mathrm{S}_{\bar{\psi}} + \mathrm{C}_{\bar{\phi}}\mathrm{C}_{\bar{\psi}}\right) & \alpha_{131}\mathrm{S}_{\bar{\phi}}\mathrm{C}_{\bar{\theta}} \\ \alpha_{111}\left(\mathrm{C}_{\bar{\phi}}\mathrm{S}_{\bar{\theta}}\mathrm{C}_{\bar{\psi}} + \mathrm{S}_{\bar{\phi}}\mathrm{S}_{\bar{\psi}}\right) & \alpha_{121}\left(\mathrm{C}_{\bar{\phi}}\mathrm{S}_{\bar{\theta}}\mathrm{S}_{\bar{\psi}} - \mathrm{S}_{\bar{\phi}}\mathrm{C}_{\bar{\psi}}\right) & \alpha_{131}\mathrm{C}_{\bar{\phi}}\mathrm{C}_{\bar{\theta}} \end{bmatrix}$$

$$\mathrm{K}_{\text{P1}}(t) = -B_1^{-1}\left(\bar{\mathbf{\Gamma}}_0\right)A_{1\bullet 2}$$
$$= \begin{bmatrix} \alpha_{112}\mathrm{C}_{\bar{\theta}}\mathrm{C}_{\bar{\psi}} & \alpha_{122}\mathrm{C}_{\bar{\theta}}\mathrm{S}_{\bar{\psi}} & -\alpha_{132}\mathrm{S}_{\bar{\theta}} \\ \alpha_{112}\left(\mathrm{S}_{\bar{\phi}}\mathrm{S}_{\bar{\theta}}\mathrm{C}_{\bar{\psi}} - \mathrm{C}_{\bar{\phi}}\mathrm{S}_{\bar{\psi}}\right) & \alpha_{122}\left(\mathrm{S}_{\bar{\phi}}\mathrm{S}_{\bar{\theta}}\mathrm{S}_{\bar{\psi}} + \mathrm{C}_{\phi}\mathrm{C}_{\bar{\psi}}\right) & \alpha_{132}\mathrm{S}_{\bar{\phi}}\mathrm{C}_{\bar{\theta}} \\ \alpha_{112}\left(\mathrm{C}_{\bar{\phi}}\mathrm{S}_{\bar{\theta}}\mathrm{C}_{\bar{\psi}} + \mathrm{S}_{\bar{\phi}}\mathrm{S}_{\bar{\psi}}\right) & \alpha_{122}\left(\mathrm{C}_{\bar{\phi}}\mathrm{S}_{\bar{\theta}}\mathrm{S}_{\bar{\psi}} - \mathrm{S}_{\bar{\phi}}\mathrm{C}_{\bar{\psi}}\right) & \alpha_{132}\mathrm{C}_{\bar{\phi}}\mathrm{C}_{\bar{\theta}} \end{bmatrix}$$

The total body velocity command is then

$$\mathbf{V} = \bar{\mathbf{V}} + \mathbf{V}_{\text{ctrl}}.$$

Inner Loop Guidance Control

The inner-loop, nominal guidance controller calculates the nominal force by inversion of the translational dynamics (8), using (11) to calculate $\dot{\bar{\mathbf{V}}}$. Inserting nominal values of $\mathbf{\Omega}$ as calculated at the previous time step, the result is

$$\bar{\mathbf{F}}_{\text{b}} = m\left[\dot{\bar{\mathbf{V}}} - B_2\left(\bar{\mathbf{\Omega}}_0\right)\bar{\mathbf{V}}\right]. \tag{18}$$

The tracking error of the closed-loop, translational dynamics is next defined as $\mathbf{V}_{\text{err}} = \mathbf{V}_{\text{sens}} - \mathbf{V}_{\text{com}}$, and the linearized error dynamics is written as

$$\dot{\mathbf{V}}_{\text{err}} = B_2\left(\bar{\mathbf{\Omega}}_0\right)\mathbf{V}_{\text{err}} + \frac{1}{m}\mathbf{F}_{\text{ctrl}}. \tag{19}$$

The LTV stabilizing control law is

$$\mathbf{F}_{\text{ctrl}} = -\mathrm{K}_{\text{P2}}(t)\mathbf{V}_{\text{err}} - \mathrm{K}_{\text{I2}}(t)\int_{t_0}^{t}\mathbf{V}_{\text{err}}(\tau)\,d\tau, \tag{20}$$

and the controller gain matrices are written as

$$\mathrm{K}_{\text{P2}}(t) = m\left(B_2\left(\bar{\mathbf{\Omega}}_0\right) - A_{2\bullet 2}\right)$$
$$= m\begin{bmatrix} \alpha_{212} + C_{xu} & \bar{r} & -\bar{q} \\ -\bar{r} & \alpha_{222} + C_{yu} & \bar{p} \\ \bar{q} & -\bar{p} & \alpha_{232} + C_{zu} \end{bmatrix}$$

$$\mathrm{K}_{\text{I2}}(t) = -mA_{2\bullet 1} = m\begin{bmatrix} \alpha_{211} & 0 & 0 \\ 0 & \alpha_{221} & 0 \\ 0 & 0 & \alpha_{231} \end{bmatrix}.$$

The total commanded force is thus $\mathbf{F}_{\text{com}} = \bar{\mathbf{F}}_{\text{b}} + \mathbf{F}_{\text{b,ctrl}}$.

3) Control Allocation

The TLC algorithm yields both a nominal force component $\bar{\mathbf{F}}_{\text{b}}$ in the open-loop feedforward path, and a closed-loop feedback control component $\mathbf{F}_{\text{b,ctrl}}$ calculated by the LTV tracking-error controller. Allocation is performed separately for the nominal and total ($\bar{\mathbf{F}}_{\text{b}} + \mathbf{F}_{\text{b,ctrl}}$) commands to avoid unnecessary feedback loops in the feedforward controller.

Nominal Guidance Control Allocation

The nominal guidance allocation takes $\bar{\mathbf{F}}_{\text{b}}$ as input and calculates the thrust coefficient $\bar{\delta}_\tau$, and the virtual controls $\bar{\alpha}$ and $\bar{\beta}$ required at the next time step to track the nominal trajectory. Values from the previous time-step $(\bar{\alpha}_0, \bar{\beta}_0)$ are used to generate the aerodynamic and thrust commands by inversion of the force model (1) - (3).

The total force on the aircraft can be written as a sum of aerodynamic, thrust, and gravitational forces. Using the engine and control surfaces, some of these components can be adjusted, but some cannot. It is not possible to completely eliminate the drag force no matter what the vehicle orientation, and so a baseline value is chosen as the drag experienced at zero-alpha, zero-beta. The zero-alpha lift value is defined similarly, and these base values are subtracted from the total nominal force prior to allocation.

A bank-to-turn (BTT) approach is adopted in this design to minimize undesirable sideslip, and this maneuver involves rolling the aircraft and aligning the lift vector to provide the centripetal acceleration. This then requires increased

elevator to offset the loss of lift and increased g-force in the turn, as well as some rudder to maintain heading angle. The control allocation design uses the virtual controls α and β to realize the lift and sideforce, and calculates the required thrust coefficient δ_τ based on those results. The aerodynamic coefficients are converted to the body-frame, and forces are approximated as

$$F_{x,\mathrm{a}} + T = QSC_{X_0} + QSC_{X_\alpha}\alpha + QSC_{X_\beta}\beta + T_{\max}\delta_\tau \tag{21}$$

$$F_{y,\mathrm{a}} = QSC_{Y_\beta}\beta + QSC_{Y_{\delta r}}\delta_r \tag{22}$$

$$F_{z,\mathrm{a}} = QSC_{Z_0} + QSC_{Z_\alpha}\alpha + QSC_{Z_{\delta e}}\delta_e, \tag{23}$$

and the nominal gravitational components are subtracted out along with components due zero-alpha aerodynamics. The remaining forces are dependent on the states being controlled, and care is taken to avoid introducing unnecessary feedback paths in the nominal open-loop controller. The lift and side forces are allocated to α and β as

$$\bar{\alpha} = \frac{\bar{Z} - \bar{Q}SC_{Z_0}}{\bar{Q}SC_{Z_\alpha}} \tag{24}$$

$$\bar{\beta} = \frac{\bar{Y}}{\bar{Q}SC_{Y_\beta}}, \tag{25}$$

and the thrust force is allocated to the thrust coefficient using

$$\bar{\delta}_\tau = \frac{\bar{F}_\alpha - \bar{Q}SC_{X_0} - \bar{Q}SC_{X_\alpha}\bar{\alpha} - \bar{Q}SC_{X_\beta}\bar{\beta}}{T_{\max}}. \tag{26}$$

Nominal Euler Angles

The nominal Euler angles are obtained by simultaneously satisfying roll-angle and rate-of-climb constraints [34]. The roll angle is given by

$$\bar{\phi} = \tan^{-1}\left(\Upsilon_{\mathrm{com}} \frac{\cos\bar{\beta}}{\cos\bar{\alpha}} \frac{\left(a - b^2\right) + b\tan\bar{\alpha}\sqrt{c\left(1-b^2\right) + \Upsilon_{\mathrm{com}}^2 \sin^2\bar{\beta}}}{a^2 - b^2\left(1 + c\tan^2\bar{\alpha}\right)} \right)$$

where

$$a = 1 - \Upsilon_{\mathrm{com}}\tan\bar{\alpha}\sin\bar{\beta}, \quad b = \frac{\sin\bar{\gamma}}{\cos\bar{\beta}}, \quad c = 1 + \Upsilon_{\mathrm{com}}^2\cos^2\bar{\beta}$$

and

$$\Upsilon_{\mathrm{com}} \equiv \frac{\dot{\chi}_{\mathrm{com}} V_{T,\mathrm{com}}}{g}.$$

The required pitch-angle $\bar{\theta}$ is obtained next using the rate-of-climb constraint equation given by

$$\bar{\theta} = \tan^{-1}\frac{ab + \sin\bar{\gamma}\sqrt{a^2 - \sin^2\bar{\gamma} + b^2}}{a^2 - \sin^2\bar{\gamma}}, \quad \bar{\theta} \neq \pm\frac{\pi}{2}$$

where

$$a = \cos\bar{\alpha}\cos\bar{\beta},$$

and

$$b = \sin\bar{\phi}\sin\bar{\beta} + \cos\bar{\phi}\sin\bar{\alpha}\cos\bar{\beta}.$$

The yaw angle $\bar{\psi}$ is obtained by first calculating the bank angle as an intermediate variable using

$$\bar{\sigma} = \tan^{-1}\left(\frac{\bar{u}\bar{v}\sin\bar{\theta} + \left(\bar{u}^2 + \bar{w}^2\right)\sin\bar{\phi}\cos\bar{\theta} - \bar{v}\bar{w}\cos\bar{\phi}\cos\bar{\theta}}{V_{t,\mathrm{com}}\left(\bar{w}\sin\bar{\theta} + \bar{u}\cos\bar{\phi}\cos\bar{\theta}\right)} \right),$$

and then finally

$$\bar{\psi} = \tan^{-1}\left\{ \frac{\Psi_1\cos\chi_{\mathrm{com}} + \Psi_2\sin\chi_{\mathrm{com}}}{-\Psi_3\sin\chi_{\mathrm{com}} + \Psi_4\cos\chi_{\mathrm{com}}} \right\}, \tag{27}$$

where

$$\Psi_1 = \left(\sin\bar{\sigma}\sin\bar{\alpha} - \cos\bar{\alpha}\cos\bar{\sigma}\sin\bar{\beta}\right)$$

$$\Psi_2 = \left[\cos\bar{\gamma}\cos\bar{\alpha}\cos\bar{\beta} - \sin\bar{\gamma}\left(\sin\bar{\alpha}\cos\bar{\sigma} + \sin\bar{\beta}\cos\bar{\alpha}\sin\bar{\sigma}\right)\right]$$

$$\Psi_3 = \left(\sin\bar{\sigma}\sin\bar{\alpha} - \cos\bar{\alpha}\cos\bar{\sigma}\sin\bar{\beta}\right)$$

$$\Psi_4 = \cos\bar{\gamma}\cos\bar{\alpha}\cos\bar{\beta} - \sin\bar{\gamma}\left(\sin\bar{\alpha}\cos\bar{\sigma} + \sin\bar{\beta}\cos\bar{\alpha}\sin\bar{\sigma}\right).$$

B. Attitude Tracking Control

The attitude loop controller is shown as Loops 3 and 4 in Figure 3. The nominal moments required to achieve the desired attitudes are calculated in the upper path, and feedback control is performed in the lower path. The outputs of the nominal and feedback controllers are summed and passed to the attitude allocation subsystem.

1) Outer Loop Attitude Control

Outer loop, nominal attitude control is achieved starting with dynamic inversion of the rotational kinematics equations (10), followed by evaluation at the nominal flight condition, giving

$$\bar{\boldsymbol{\Omega}} = B_3^{-1}\left(\bar{\boldsymbol{\Gamma}}_0\right)\dot{\bar{\boldsymbol{\Gamma}}}. \tag{28}$$

The Euler angle tracking error is next defined as $\boldsymbol{\Gamma}_{\mathrm{err}} = \boldsymbol{\Gamma}_{\mathrm{sens}} - \boldsymbol{\Gamma}_{\mathrm{com}}$, with the linearized tracking error dynamics given by

$$\dot{\boldsymbol{\Gamma}}_{\mathrm{err}} = B_3\left(\bar{\boldsymbol{\Gamma}}_0\right)\boldsymbol{\Omega}_{\mathrm{ctrl}}. \tag{29}$$

The PI control law for the attitude outer-loop is written as

$$\boldsymbol{\Omega}_{\mathrm{ctrl}} = -\mathrm{K}_{\mathrm{P3}}(t)\boldsymbol{\Gamma}_{\mathrm{err}} - \mathrm{K}_{\mathrm{I3}}(t)\int_{t_0}^{t}\boldsymbol{\Gamma}_{\mathrm{err}}(\tau)\,d\tau \tag{30}$$

with the controller gain matrices synthesized as

$$\mathrm{K}_{\mathrm{P3}}(t) = \begin{bmatrix} \alpha_{312} & \bar{q}\mathrm{S}_{\bar{\phi}} + \bar{r}\mathrm{C}_{\bar{\phi}} & -\alpha_{332}\mathrm{S}_{\bar{\theta}} \\ -\bar{r} & \alpha_{322}\mathrm{C}_{\bar{\phi}} + \left(\mathrm{S}_{\bar{\theta}}\left[\bar{q}\mathrm{S}_{\bar{\phi}} + \bar{r}\mathrm{C}_{\bar{\phi}}\right]\mathrm{S}_{\bar{\phi}}/\mathrm{C}_{\bar{\theta}}\right) & \alpha_{332}\mathrm{S}_{\bar{\phi}}\mathrm{C}_{\bar{\theta}} \\ \bar{q} & -\alpha_{322}\mathrm{S}_{\bar{\phi}} + \left(\mathrm{S}_{\bar{\theta}}\left[\bar{q}\mathrm{S}_{\bar{\phi}} + \bar{r}\mathrm{C}_{\bar{\phi}}\right]\mathrm{C}_{\bar{\phi}}/\mathrm{C}_{\bar{\theta}}\right) & \alpha_{332}\mathrm{C}_{\bar{\phi}}\mathrm{C}_{\bar{\theta}} \end{bmatrix}$$

$$\mathrm{K}_{\mathrm{I3}}(t) = \begin{bmatrix} \alpha_{311} & 0 & -\alpha_{331}\mathrm{S}_{\bar{\theta}} \\ 0 & -\alpha_{321}\mathrm{C}_{\bar{\phi}} & \alpha_{331}\mathrm{S}_{\bar{\phi}}\mathrm{C}_{\bar{\theta}} \\ 0 & -\alpha_{321}\mathrm{S}_{\bar{\phi}} & \alpha_{331}\mathrm{C}_{\bar{\phi}}\mathrm{C}_{\bar{\theta}} \end{bmatrix}.$$

2) Inner Loop Attitude Control

Inner loop control starts with dynamic inversion of the rotational dynamics equation (10), giving

$$\bar{\mathbf{T}}_m = B_4^{-1}\left[\dot{\bar{\boldsymbol{\Omega}}} - f_4\left(\bar{\boldsymbol{\Omega}}\right)\right]. \tag{31}$$

The body-rate error is defined next as $\boldsymbol{\Omega}_{\mathrm{err}} = \boldsymbol{\Omega}_{\mathrm{sens}} - \boldsymbol{\Omega}_{\mathrm{com}}$, and the PI control law for the attitude inner loop is written as

$$\mathbf{T}_{\mathrm{m,ctrl}} = -\mathrm{K}_{\mathrm{P4}}(t)\boldsymbol{\Omega}_{\mathrm{err}} - \mathrm{K}_{\mathrm{I4}}(t)\int_{t_0}^{t}\boldsymbol{\Omega}_{\mathrm{err}}(\sigma)\,d\sigma. \tag{32}$$

The 3 × 3 controller gain matrices are given by

$$k_{\mathrm{P4},11}(t) = I_{xx}\left(\alpha_{412} + I^{p}_{pq}\overline{q}\right) - I^{r}_{pq}I_{xz}\overline{q} + L_p$$
$$k_{\mathrm{P4},21}(t) = I_{yy}\left(2I^{q}_{pp}\overline{p} + I^{q}_{pr}\overline{r}\right)$$
$$k_{\mathrm{P4},31}(t) = -I_{xz}\left(I^{p}_{pq}\overline{q} + \alpha_{412}\right) + I_{zz}I^{r}_{pq}\overline{q} + N_p$$
$$k_{\mathrm{P4},12}(t) = I_{xx}\left(I^{p}_{pq}\overline{p} + I^{p}_{pr}\overline{r}\right) - I_{xz}\left(I^{r}_{pq}\overline{p} + I^{r}_{qr}\overline{r}\right)$$
$$k_{\mathrm{P4},22}(t) = \alpha_{422}I_{yy} + M_q$$
$$k_{\mathrm{P4},23}(t) = -I_{xz}\left(I^{p}_{pq}\overline{p} + I^{p}_{qr}\overline{r}\right) + I_{zz}\left(I^{r}_{pq}\overline{p} + I^{r}_{qr}\overline{r}\right)$$
$$k_{\mathrm{P4},31}(t) = I_{xx}I^{p}_{qr}\overline{q} - I_{xz}\left(I^{r}_{qr}\overline{q} + \alpha_{432}\right) + L_r$$
$$k_{\mathrm{P4},32}(t) = I_{yy}\left(2I^{q}_{rr}\overline{r} + I^{q}_{pr}\overline{p}\right)$$
$$k_{\mathrm{P4},33}(t) = -I_{xz}I^{p}_{qr}\overline{q} + I_{zz}\left(I^{r}_{qr}\overline{q} + \alpha_{432}\right) + N_r$$

$$\mathrm{K}_{\mathrm{I4}}(t) = \begin{bmatrix} I_{xx}\alpha_{411} & 0 & -I_{xz}\alpha_{431} \\ 0 & I_{yy}\alpha_{421} & 0 \\ -I_{xz}\alpha_{411} & 0 & I_{zz}\alpha_{431} \end{bmatrix},$$

and the total output of the attitude controller is

$$\mathbf{T}_{\mathrm{m,com}} = \overline{\mathbf{T}}_{\mathrm{m}} - \mathbf{T}_{\mathrm{m,ctrl}}. \tag{33}$$

C. Attitude Control Allocation

Control surface deflections that will generate the commanded moments are calculated by the attitude allocation subsystem. Allocation is performed by inverting the torque model given by (4) - (6) at $\mathbf{T}_{\boldsymbol{m},\mathrm{com}}$, α_{com}, and β_{com}. The moment equations are then written in terms of the Jacobian, so that

$$\begin{bmatrix} L_{m,\mathrm{com}} - QSbC_{l_\beta}\beta_{\mathrm{com}} \\ M_{m,\mathrm{com}} - QS\overline{c}\left(C_{m_0} + C_{m_\alpha}\alpha_{\mathrm{com}}\right) \\ N_{m,\mathrm{com}} - QSbC_{n_\beta}\beta_{\mathrm{com}} \end{bmatrix} \begin{bmatrix} QSbC_{l_{\delta a}} & 0 & QSbC_{l_{\delta r}} \\ 0 & QS\overline{c}C_{m_{\delta_e}} & 0 \\ QSbC_{n_{\delta a}} & 0 & QSbC_{n_{\delta r}} \end{bmatrix} = \begin{bmatrix} \delta_{a,\mathrm{com}} \\ \delta_{e,\mathrm{com}} \\ \delta_{r,\mathrm{com}} \end{bmatrix}$$

$$U = J_2^{-1} = \begin{bmatrix} QSbC_{l_{\delta a}} & 0 & QSbC_{l_{\delta r}} \\ 0 & QS\overline{c}C_{m_{\delta_e}} & 0 \\ QSbC_{n_{\delta a}} & 0 & QSbC_{n_{\delta r}} \end{bmatrix}^{-1}$$

and inversion gives the effector setting commands

$$\begin{bmatrix} \delta_{a,\mathrm{com}} \\ \delta_{e,\mathrm{com}} \\ \delta_{r,\mathrm{com}} \end{bmatrix} = U \begin{bmatrix} L_{m,\mathrm{com}} - QSbC_{l_\beta}\beta_{\mathrm{com}} \\ M_{m,\mathrm{com}} - QS\overline{c}\left(C_{m_0} + C_{m_\alpha}\alpha_{\mathrm{com}}\right) \\ N_{m,\mathrm{com}} - QSbC_{n_\beta}\beta_{\mathrm{com}} \end{bmatrix}. \tag{34}$$

IV. Tests & Simulation Results

The 6DOF controller and single-engine aircraft dynamics model are implemented using the nonlinear equations of motion (7) - (10), the aerodynamic force/torque model given by (1) - (6), and a proportional thrust law $T = T_{\max}\delta_\tau$. The twelve aircraft states, given by

$$\left(x_e \quad y_e \quad z_e \quad u \quad v \quad w \quad \phi \quad \theta \quad \psi \quad p \quad q \quad r\right),$$

are tracked, and each of the three control surfaces and the constant speed propeller are implemented with actuator dynamics given by

$$G(s) = \frac{10}{s+10}. \tag{35}$$

Referring back to Figure 3, the 6DOF controller and aircraft model are implemented using MATLAB/Simulink. Each of the four control loops shown in the figure are constructed similarly, and consist of a dynamic pseudo-inverse, and an LTV tracking-error controller. Nominal trajectory tracking is tested using a climbing, coordinated-turn command. Controller parameters are given in Tables 1 and 2, and simulation results are given in Figure 4 – 9

Table 1. TLC Guidance Loop Controller Parameters

	outer loop ($i=1$)			inner loop ($i=2$)		
	x	y	z	u	v	w
ω_n	0.075	0.005	0.098	0.390	0.036	0.390
ζ_n	1.414	1.414	1.414	1.414	1.414	1.414
$\omega_{n,\mathrm{diff}}$	1.250	1.250	1.250	5.000	5.000	5.000
$\zeta_{n,\mathrm{diff}}$	1.414	1.414	1.414	1.414	1.414	1.414

Table 2. TLC Attitude Loop Controller Parameter

	outer loop ($i=3$)			inner loop ($i=4$)		
	ϕ	θ	ψ	p	q	r
ω_n	0.600	2.200	0.600	9.600	9.600	6.000
ζ_n	1.414	1.414	1.414	2.82	1.414	1.414
$\omega_{n,\mathrm{diff}}$	20.00	20.00	20.00	80.00	96.00	80.00
$\zeta_{n,\mathrm{diff}}$	1.414	1.414	1.414	1.414	1.414	1.414

In the simulation, the aircraft is initially flying at a trim condition, with $V_{t,\mathrm{com}} = 165$ ft/s, and $\gamma_{\mathrm{com}} = \chi_{\mathrm{com}} = 0°$. A climbing, 360º turn is commanded at $t = 200s$, with commanded turn-rate $\dot{\chi}_{\mathrm{com}} = 1\,deg/s$ and commanded flight path angle $\gamma_{\mathrm{com}} = 1°$. After a full circle the overall command returns to straight and level. Figure 4 is a 3D plot of the commanded and actual aircraft trajectories. Figures 5-9 show the time history of the twelve state-variables, as well as the velocity magnitude, flight path angle, and heading angle. In the figures, the solid blue lines are the nominal commands (the results of the pseudoinversion), the red dot-dashed lines are the *total* commands (nominal plus feedback control), and the green dotted lines are the calculated vehicle response. The figures show that all of the vehicle states are tracked closely throughout the duration of the maneuver. Also, the velocity magnitude remains constant to within less than 2 ft/s, and the flight path and heading angles track very closely.

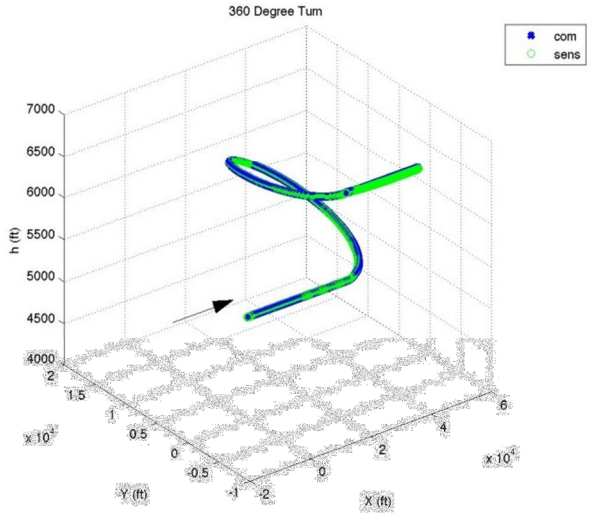

Figure 4. 360º Climbing Turn: Trajectory Tracking

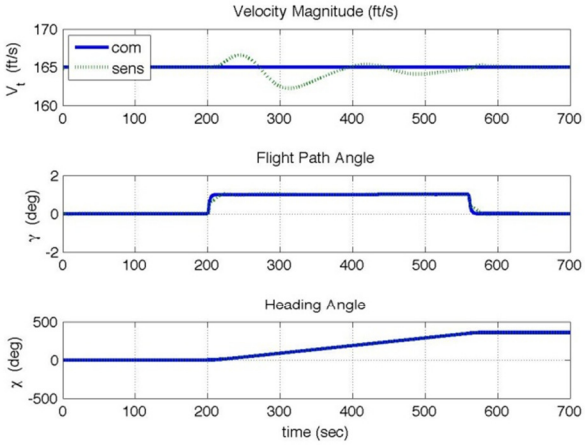

Figure 5. Velocity Magnitude, Flight Path & Heading Angles

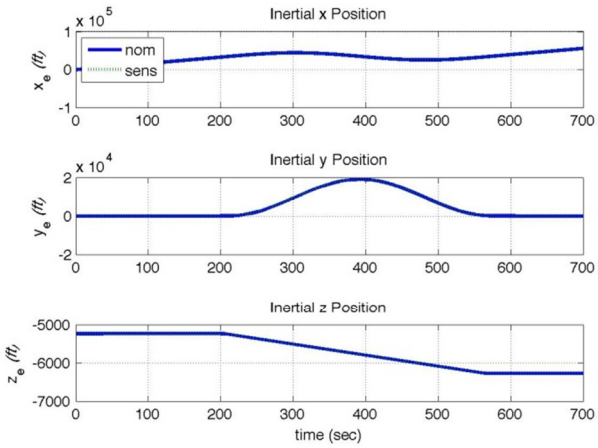

Figure 6. Inertial Position Tracking

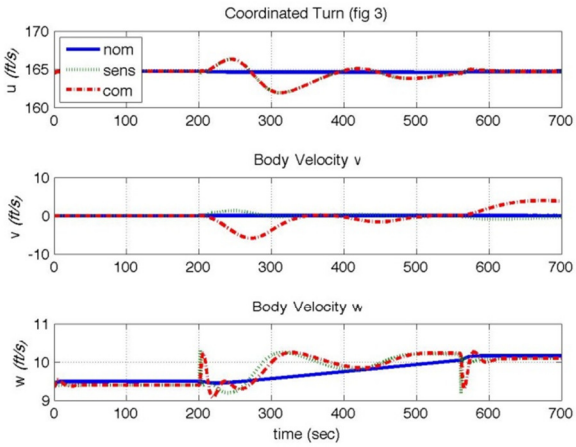

Figure 7. Body Velocity Tracking

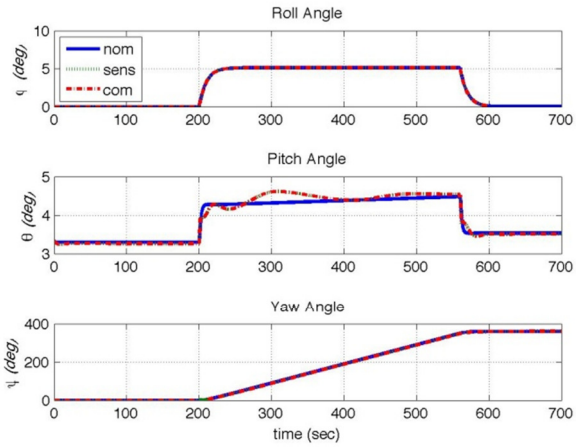

Figure 8. Attitude Tracking

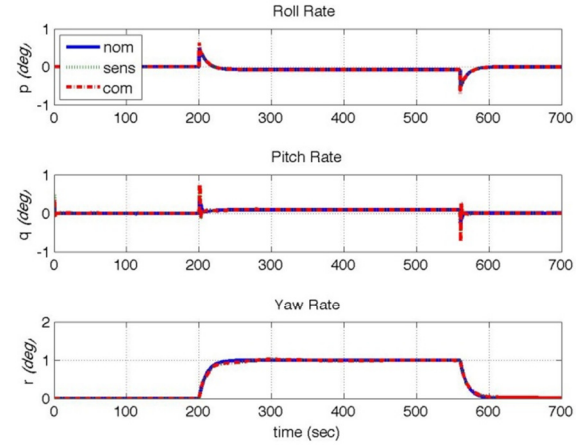

Figure 9. Body Rate Tracking

V. CONCLUSION

This paper describes an autonomous, 6DOF, trajectory-tracking flight control design for a fixed-wing aircraft flight dynamics model. Forces and moments are calculated using standard build-up methods, and coefficients have been

obtained for a typical general aviation (such as a Cessna 182) from the literature. The TLC controller generates a nominal twelve-state trajectory, and calculates nominal force and torque commands by dynamic inversion of the nonlinear equations of motion. An LTV tracking error regulator provides robustness to model uncertainty and error. Control allocation is performed by inversion of the force/torque model using nominal guidance, feedback guidance, and attitude components. Nominal trajectory results have been presented for a climbing, 360º, bank-to-turn maneuver showing the effectiveness of the TLC design.

REFERENCES

[1] Ippolito, C.A, and Yeh, Y.H., "A Trajectory Generation Approach for Payload Directed Flight," 47th AIAA Aerospace Sciences Meeting Including The New Horizons Forum and Aerospace Exposition, AIAA Paper 2009-1351, Jan. 2009.

[2] Croft, J. W., "Refuse to Crash: NASA Tackles Loss of Control." AIAA - Aerospace America Online, March 2004.

[3] Adami, T.A., and Zhu, J.J., "Control of a Flexible, Hypersonic Scramjet Vehicle Using a Differential Algebraic Approach," AIAA Guidance, Navigation and Control Conference and Exhibit, AIAA Paper 2008-7464, Aug. 2008.

[4] Lawrence, D., Rugh, W., "Gain Scheduling Dynamic Linear Controllers Nonlinear Plant," Automatica, Vol. 31, No. 3, pp. 38-390, 1995.

[5] Rugh, W.J., Shamma, J.S., "Research on Gain Scheduling," Automatica 36 (2000) 1401-1425.

[6] Fromion, V., Scorletti, G., "A Theoretical Framework for Gain Scheduling," Int. J. Robust Nonlinear Control 2003; 13:951–982.

[7] Marcos, A., Balas, G.J., "Development of Linear-Parameter-Varying Models for Aircraft," Journal Of Guidance, Control, And Dynamics, Vol. 27, No. 2, March-April 2004.

[8] Atsushi Fujimori, A., Tsunetomo, H., Wu, Z-Y., "Gain-Scheduled Control Using Fuzzy Logic and Its Application to Flight Control," J. Guidance, Vol. 22, No. 1: Engineering Notes, 1997.

[9] Nichols, R. A., Reichert, R.T., Rugh, W.J., "Gain scheduling control for H-Infinity controllers: a flight control example," IEEE Trans. Contro Syst. Technol., 1, 69-75, 1993.

[10] Enns, D., Bugajski, D., Hendrick, R., Stein, G., "Dynamic inversion: an evolving methodology for flight control design," Vol. 59, No. 1, 71-91, 1994.

[11] Smith, G.A., Meyert, G., "Aircraft Automatic Flight Control System with Model Inversion," Vol. 10, No. 3, May-June 1987 J. Guidance.

[12] Snell, S.A., "Nonlinear Inversion Flight Control for a Super-maneuverable Aircraft," Journal of Guidance, Control, and Dynamics, Vol. 15, No. 4. July-Aug 1992, 976-984.

[13] Honeywell, Lockheed, AFRL, "Application Of Multivariable - Control Theory To Aircraft Control Laws," WL-TR-96-3099, May 1996.

[14] Shapiro, E.Y., Chung, J.C., "Flight Control System Synthesis Using Eigenstructure Assignment," Shapiro, E.Y., Chung, J.C., Journal Of Optimization Theory And Applications: Vol. 43, No. 3, July 1984.

[15] Franklin, S. N., Ackermann, J, "Robust Flight Control: A Design Example," J. Guidance and Control Vol. 4, No. 6, Nov.-Dec. 1981, 597-605. AIAA 81-4308.

[16] Wang, Q., Stengel, R.F., "Robust Nonlinear Flight Control of a High-Performance Aircraft," IEEE Transactions on Control Systems Technology, Vol. 13, No. 1, January 2005.

[17] Johnson, E., Calise, A., and Corban, J.E., "A Six Degree-of-Freedom Adaptive Flight Control Architecture for Trajectory Following", AIAA Guidance, Navigation, and Control Conference and Exhibit, AIAA Paper 2002-4776, Aug. 2002.

[18] Lee, T., Kim, Y., "Nonlinear Adaptive Flight Control Using Backstepping and Neural Networks Controller," Journal of Guidance, Control, and Dynamics, Vol. 24, No. 4, July-August 2001, pp 675-682.

[19] Kim, A., and Calise, A, "Nonlinear Flight Control Using Neural Networks ", Journal of Guidance, Control, and Dynamics, Vol. 20, No. 1, 1997, pp. 26-33.

[20] Kanishege, J., Bull, J. and Totah, J., "Generic Neural Flight Control and Autopilot System," AIAA 2000-4281, August 2000.

[21] Sahjendra N. Singh, S.N., Steinberg, M.L., Page, A.B., "Nonlinear Adaptive and Sliding Mode Flight Path Control of F/A-18 Model," IEEE Transactions On Aerospace And Electronic Systems Vol. 39, No. 4 October 2003.

[22] MacKunis, W., Kaiser, M.K., "Adaptive Dynamic Inversion for Asymptotic Tracking of an Aircraft Reference Model," AIAA Guidance, Navigation and Control Conference and Exhibit, 18 - 21 August 2008, Honolulu, Hawaii, AIAA 2008-6792.

[23] Cabecinhas, D., Silvestre, C., Rosa, P., and Cunha, R., "Path-Following Control for Coordinated Turn Aircraft Maneuvers," AIAA Guidance, Navigation and Control Conference and Exhibit, AIAA Paper 2007-6656, 2007.

[24] Zhu, J., Banker, B. D., and Hall, C. E., "X-33 Ascent Flight Controller Design By Trajectory Linearization - A Singular Perturbational Approach," AIAA Guidance, Navigation and Control Conference and Exhibit, AIAA Paper 2000-4159, Aug. 2000.

[25] Zhu, J "PD-spectral theory for multivariable linear time-varying systems," Proc. The 46th IEEE CDC, San Diego, CA Dec 1997, pp. 3908-3913.

[26] Zhu, J.J., Nonlinear Tracking and Decoupling by Trajectory Linearization, Lecture Note, June, 1998.

[27] Zhu, J., Hodel, A. S., Funston, K., and Hall, C. E., "X-33 Entry Flight Controller Design by Trajectory Linearization- a Singular Perturbational Approach," Proceedings of American Astro. Soc. G&C Conf., 2001, 11-170.

[28] Wu, X., Liu, Y. and Zhu, J. J., "Design and Real-Time Testing of a Trajectory Linearization Flight Controller for the Quanser UFO", Proceedings of American Control Conference, Denver, CO, 2003, pp.3931-3938.

[29] Huang, R., Liu, Y., Zhu, J.J., " Guidance, Navigation, and Control System Design for Tripropeller Vertical-Takeoff-and-Landing Unmanned Air Vehicle," Journal of Aircraft, Vol. 46, No. 6, November–December 2009.

[30] Adami, T.A., Zhu, J.J., Bolender, M.A., Doman, D.B., Oppenheimer, M., "Flight Control of Hypersonic Scramjet Vehicles Using a Differential Algebraic Approach," AIAA Guidance, Navigation, and Control Conference and Exhibit, 21 - 24 August 2006, Keystone, Colorado, AIAA 2006-6559.

[31] Liu, Yong, Zhu, J. "Regular Perturbation Analysis for Trajectory Linearization Control," American Control Conference, New York, 2007.

[32] Mickle, M., Zhu, J., "A Nonlinear Roll-Yaw Missile Autopilot Based on Plant Inversion and PD-Spectral Assignment," Proc. Of the 37th IEEE Conference on Decision and Control, Tampa, FL 1998.

[33] Roskam, J., Airplane Flight Dynamics and Automatic Flight Controls Pt. 1. Darcorporation, 2001.

[34] Stevens, B., Lewis, F., Aircraft Control & Simulation. Wiley-Interscience; 2nd edition 2003.

APPENDIX

The moment of inertia constants used in equation (10) are defined as:

$$I_{pq}^{p} = I_{xz}\left(I_{yy} - I_{zz} - I_{xx}\right)D$$

$$I_{pp}^{q} = -\frac{I_{xz}}{I_{yy}}$$

$$I_{pq}^{r} = \left(I_{xx}I_{yy} - I_{xz}^{2} - I_{xx}^{2}\right)D$$

$$I_{qr}^{p} = \left(I_{zz}^{2} - I_{yy}I_{zz} + I_{xz}^{2}\right)D$$

$$I_{pr}^{q} = \frac{\left(I_{zz} - I_{zz}\right)}{I_{yy}}$$

$$D = \left(I_{xz}^{2} - I_{xx}I_{zz}\right)^{-1}$$

$$I_{qr}^{r} = -\frac{I_{pq}^{p}}{I_{yy}}$$

$$I_{rr}^{q} = -I_{pp}^{q}$$

$$g_{l}^{p} = -I_{zz}D$$

$$g_{n}^{p} = -I_{xz}D = g_{l}^{r}$$

$$g_{m}^{q} = \frac{1}{I_{yy}}$$

$$g_{n}^{r} = -I_{xx}D$$